

Article

A Comparison of Different Renewable-Based DC Microgrid Energy Management Strategies for Commercial Buildings Applications

Hegazy Rezk ^{1,*}, Rania M. Ghoniem ², Seydali Ferahtia ³, Ahmed Fathy ^{4,5}, Mohamed M. Ghoniem ⁶ and Reem Alkanhel ²

- ¹ Department of Electrical Engineering, College of Engineering in Wadi Alldawasir, Prince Sattam bin Abdulaziz University, Wadi Alldawasir 11991, Saudi Arabia
- ² Department of Information Technology, College of Computer and Information Sciences, Princess Nourah bint Abdulrahman University, Riyadh 11671, Saudi Arabia
- ³ Laboratoire de Génie Electrique, Department of Electrical Engineering, University of M'sila, M'Sila 28000, Algeria
- ⁴ Electrical Engineering Department, Faculty of Engineering, Jouf University, Sakaka 72388, Saudi Arabia
- ⁵ Electrical Engineering Department, Faculty of Engineering, Zagazig University, Zagazig 44519, Egypt
- ⁶ Department of Computer, Mansoura University, Mansoura 35516, Egypt
- * Correspondence: hr.hussien@psau.edu.sa

Abstract: DC microgrid systems allow commercial buildings to use locally generated energy and achieve an optimal economy efficiently. Economical and eco-friendly energy can be achieved by employing renewable energy sources. However, additional controllable sources, such as fuel cells, are required because of their reduced efficiency and fluctuated nature. This microgrid can use energy storage systems to supply transient power and enhance stability. The functioning of the microgrid and its efficiency are related to the implemented energy management strategy. In this paper, a comparison of several reported energy management strategies is fulfilled. The considered EMSs include the fuzzy logic control (FLC) strategy, the state machine control (SMC) strategy, the equivalent consumption minimization strategy (ECMS), and external energy maximization strategy (EEMS). These strategies are compared in terms of power-saving, system efficiency, and power quality specifications. The overall results confirm the ability of EEMS (high efficiency of 84.91% and economic power-saving 6.11%) and SMC (efficiency of 84.18% with high power-saving 5.07%) for stationary applications, such as building commercial applications. These strategies provide other advantages, which are discussed in detail in this paper.

Keywords: energy management strategies; DC microgrids; energy efficiency; photovoltaic; fuel cells



Citation: Rezk, H.; Ghoniem, R.M.; Ferahtia, S.; Fathy, A.; Ghoniem, M.M.; Alkanhel, R. A Comparison of Different Renewable-Based DC Microgrid Energy Management Strategies for Commercial Buildings Applications. *Sustainability* **2022**, *14*, 16656. <https://doi.org/10.3390/su142416656>

Academic Editor: George Kyriakarakos

Received: 8 November 2022

Accepted: 6 December 2022

Published: 12 December 2022

Publisher's Note: MDPI stays neutral with regard to jurisdictional claims in published maps and institutional affiliations.



Copyright: © 2022 by the authors. Licensee MDPI, Basel, Switzerland. This article is an open access article distributed under the terms and conditions of the Creative Commons Attribution (CC BY) license (<https://creativecommons.org/licenses/by/4.0/>).

1. Introduction

In recent years, numerous factors have caused an increase in energy consumption, motivating many countries to create adaptable, sustainable, affordable energy solutions [1]. In addition, the transition to clean alternative energy is required to avoid impending environmental and economic catastrophes [2]. The new energy paradigm is predicated on shifting the present power system's dependence on traditional fossil-based energy resources to an energy mix, mainly comprised of renewable energy resources (RESs) [3]. However, incorporating new RESs can bring technical and economic challenges, such as stability and financial profitability [4]. The microgrid concept based on advanced control and management technologies is the most promising solution to these issues [5]. Microgrids are a set of power sources (also called distributed generators (DGs)), including renewables, storage systems, and loads connected with control and management systems. These microgrids can be connected to the utility grid at various power and voltage levels using electronic

converters [6]. DGs may often deliver reduced generating costs, improved dependability, and increased security that traditional generators cannot. This technology expands the possibilities for efficient electric power generation, transportation, and distribution [7]. Microgrids based on RESs are located near final users to reduce transportation losses. In addition, they help reduce greenhouse gas emissions and ensure power supply during the utility grid outage [8]. Moreover, this type of power system provides an uninterrupted power supply (UPS) and is appropriate for rural and isolated areas, islands, and military applications [9]. Optimal EMS, based on the salp swarm algorithm (SSA), has been proposed in [10]. A techno-economic multi-level EMS for commercial buildings has been suggested in [11]. In this paper, the bald eagle search algorithm (BES) has been used to address operating cost minimization. An adaptive fuzzy logic controller (AFLC) has been implemented as an EMS for a DC microgrid [12], where the adaptation mechanism is based on metaheuristic optimization algorithms.

Most of the previously mentioned EMSs have been designed for electric vehicles (EVs) and off-grid applications. Updated versions of these strategies are utilized in this paper. The novelty is to modify these strategies to respond to the energy requirements of a commercial building under the grid-connected mode. The building's power system, represented in Figure 1, is based on a DC microgrid, including two sources: a photovoltaic generation unit (PV) and a fuel cell system (FC), a battery storage system, and an AC/DC grid-connection converter. Then, a comparative study between the pre-mentioned EMSs is carried out to evaluate the performance of each one in terms of efficiency, energy consumption, final storage system SoC and power quality. The main contributions of this paper can be presented as follows:

- Design-updated EMSs based on the pre-mentioned conventional EMS: FLC, SMC, ECMS, and EEMS for stationary applications such as commercial building power systems.
- Evaluate the performance of each one of the proposed EMS.
- Realization of comparative study in terms of the power-saving, system efficiency, and power quality specifications.

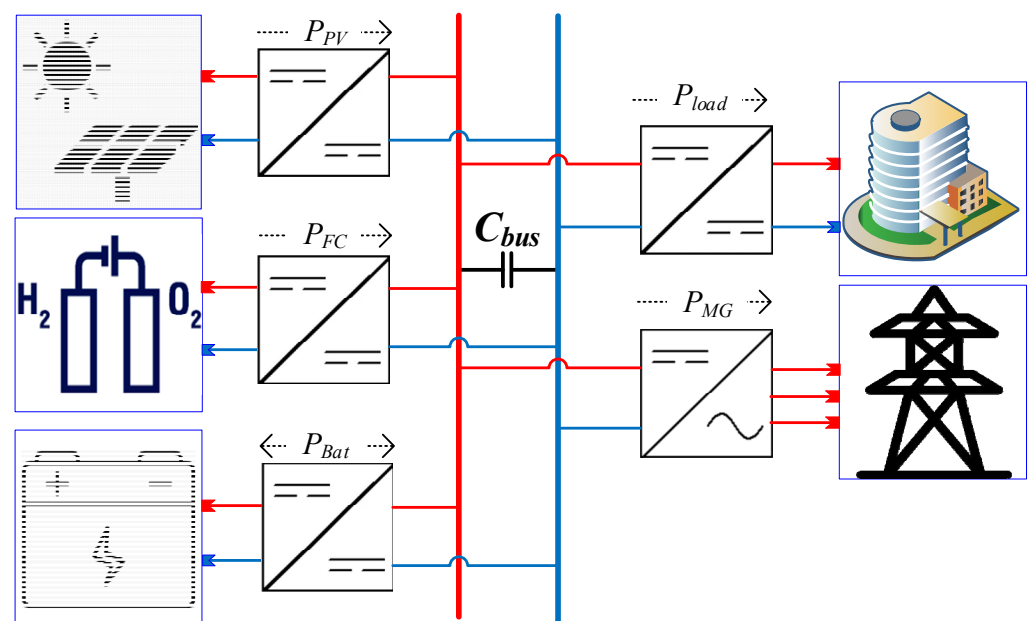


Figure 1. The architecture of the proposed DC microgrid, where all the power sources are connected to the DC bus using their converters.

2. Building Power System Modeling

2.1. Power System Description

In contrast to the alternating current (AC) building power systems that incorporate photovoltaics and DC loads, direct current (DC) power systems with modern power electronics can reduce much of the power conversion loss. According to the literature, DC microgrids can save up to 15% of electricity in buildings [13], where 308 V infrastructure microgrid voltage is the standard value [14]. The structure of the studied building's power system is illustrated in Figure 1. A fuel cell system, a photovoltaic array, and a Lithium-ion battery storage system mainly electrify the building. The microgrid can be connected to the utility grid through a bidirectional DC/AC converter. These sources are connected to the 380 V bus using their static converters.

2.2. Modeling of PV Array

Installing solar PV on commercial roofs would make good economic sense, minimizing carbon emissions and allowing unused rooftop space to be used. A single-diode equivalent circuit model is presented in Figure 2. According to [15], using the Kirchhoff Law, the governing equation of this equivalent circuit is:

$$\begin{aligned} I &= I_{ph} - I_d - I_r \\ &= I_{ph} - I_0 \underbrace{\left[e^{\frac{V+I \cdot R_s}{nV_{th}}} - 1 \right]}_{I_d} - \underbrace{\frac{V + I \cdot R_s}{R_{sh}}}_{I_r} \end{aligned} \quad (1)$$

where I_{ph} , I_d , and I_r are the photocurrent, the diode, and the shunt resistance currents, respectively; n represents the ideality factor; I_0 is the saturation current; R_s and R_{sh} are the series and parallel equivalent resistances; and V_{th} denotes the thermal voltage provided, as follows:

$$V_{th} = \frac{k \cdot T_c}{q} \quad (2)$$

where q is the elementary charge (1.602×10^{-19} C); T_c represents the cell temperature in K; and k is the Boltzmann constant (1.381×10^{-23} J/K).

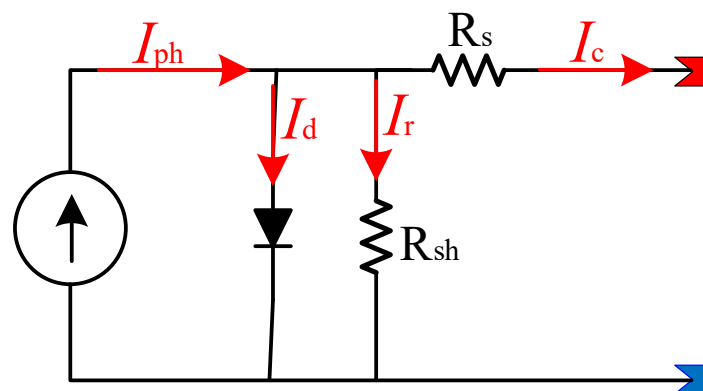


Figure 2. PV equivalent circuit.

The photocurrent is expressed as:

$$I_{ph} = \left[I_{SC} - \alpha (T_c - T_{ref}) \right] \lambda \quad (3)$$

where I_{SC} is the short circuit current in A; T_{ref} represents the measured and reference temperature in K; α is the temperature coefficient; and λ is the radiance value in kW/m^2 . There-

fore, the equation of current delivered by the PV array given in function of the number of cells in series N_S and parallel N_P can be written as:

$$I = I_{ph} - I_0 \left[e^{\frac{V_{out} + I_{out} \cdot N_S \cdot R_S}{n \cdot N_S \cdot V_{th}}} - 1 \right] - \frac{V_{out} + I_{out} \cdot N_S \cdot R_S}{R_{sh} \cdot N_S} \quad (4)$$

where V_{out} and I_{out} are the output voltage and current, respectively.

2.3. Battery Description and Modeling

Electrochemistry is employed to address the issue of intermittent renewable energy generation, as well as the sluggish dynamics of the fuel cell. The battery storage device is deployed to reduce the peak load power of the commercial building. At present, there are several types of batteries commercialized. Table 1 includes the technical information for the most popular varieties [16].

Table 1. Batteries' characteristics.

	Unit	Lead-Acid	Nickel-Metal	Nickel-Cadmium	Lithium-Ion
Cell voltage	V	2	1.25	1.25	3.6
Energy density	Wh/Kg	30–50	60–120	45–80	110–160
Power density	W/Kg	180	250–1000	150	1800
Overcharge/deep-discharge tolerance		Not tolerant	Good	Moderate	Excellent
Self-discharge rate		Low	High	Moderate	Neglected
Number of cycles		200–300	300–500	1500	500–1000

The model used in this study is a lithium-ion based on the Thevenin model [17], illustrated in Figure 3. This model is one of the most common battery models. It is based on an internal resistance model used in Matlab with a parallel RC network. It consists mainly of three components: the open-circuit voltage U_{oc} , the internal resistances, and equivalent capacitances. The internal resistances combine the ohmic resistance R_0 and the polarization resistance R_{Th} . The equivalent capacitance C_{Th} defines the battery dynamics during charging and discharging. U_{Th} is the voltage across C_{Th} .

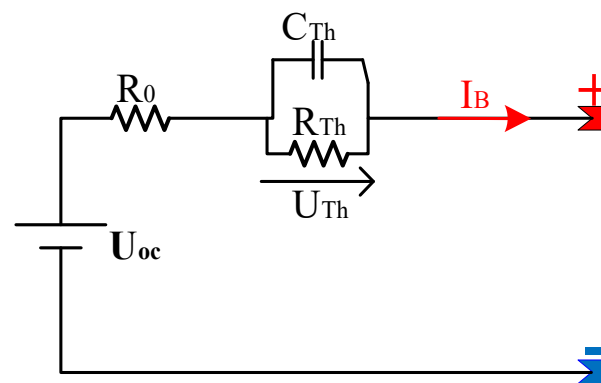


Figure 3. Li-ion battery equivalent circuit.

The source of the voltage is defined as:

$$\begin{aligned} U_B &= U_{oc} - R_0 \cdot I_B - U_{Th} \\ \dot{U}_{Th} &= -\frac{U_{Th}}{R_{Th} \cdot C_{Th}} + \frac{I_B}{C_{Th}} \end{aligned} \quad (5)$$

2.4. SOFC Description and Modeling

As reported in [18], Solid Oxide Fuel Cells (SOFCs) have excellent characteristics, deeming them the most convenient choice for stationary applications. In a SOFC, the electrolyte separates the two electrodes, creating two boundary layers. The polarization effect can charge these layers, identified as the electrochemical double-layer charging effect [19]. According to [20], the SOFC single-cell model, based on its V-I and P-I characteristics curves (Figure 4), is given as:

$$U_{FC,cell} = U_{oc} - U_{act} - U_{cons} - U_{ohm} \quad (6)$$

where U_{oc} presents the open-circuit voltage; U_{act} is the activation voltage loss; U_{cons} is the concentration voltage loss; and U_{ohm} is the ohmic voltage loss.

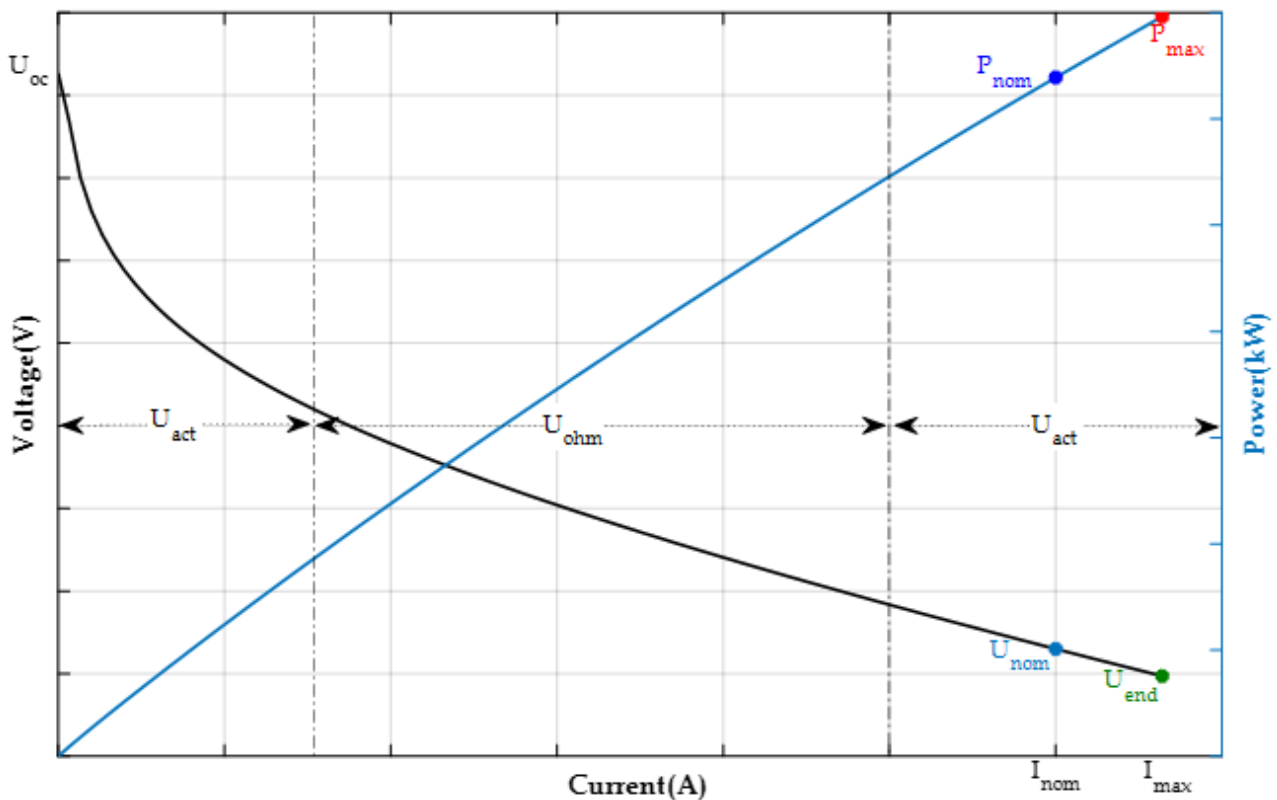


Figure 4. V-I and P-I characteristics curves.

According to [21], the open-circuit voltage and the losses voltage are given as:

$$U_{oc} = U_0 + \frac{RT}{2F} \ln \left[\frac{P_{H_2} \cdot P_{O_2}^{0.5}}{P_{H_2O}} \right] \quad (7)$$

where R and F express the universal gas constant ($8.314 \text{ KJ} (\text{mol} \cdot \text{K})^{-1}$) and Faraday constant ($96,486 \text{ } \$\text{C} \cdot \text{mol}^{-1}$), respectively. P_{H_2} , P_{O_2} , and P_{H_2O} are the partial pressures of hydrogen, oxygen, and water. T is the cell's temperature. E_0 represents the standard potential can be calculated as follows [22]:

$$U_0 = E_{std} + \frac{\Delta s}{nF} (T - 298) \quad (8)$$

where E_{std} is the voltage value under the standard conditions; n represents the number of electrons transported for each fuel molecule involved in the reaction; and Δs denotes entropy change.

The partial pressures of hydrogen, oxygen, and water formulas are reported as follows:

$$P_{H_2} = \frac{k_{H_2}^{-1}}{1 + s \cdot \tau_{H_2}} (q_{H_2}^{in} - 2 \cdot k_r \cdot I) \quad (9)$$

$$P_{O_2} = \frac{k_{O_2}^{-1}}{1 + s \cdot \tau_{O_2}} (q_{O_2}^{in} - k_r \cdot I) \quad (10)$$

$$P_{H_2O} = \frac{k_{H_2O}^{-1}}{1 + s \cdot \tau_{H_2O}} (2 \cdot k_r \cdot I) \quad (11)$$

where τ_{H_2} , τ_{O_2} , and τ_{H_2O} are the hydrogen, oxygen, and water dynamic constants; k_r is a constant that represents the reaction molar flow rate at the anode.

The activation losses can be represented using the Butler-Volmer equation [23], as follows:

$$\begin{aligned} U_{act} &= \frac{2 \cdot R \cdot T}{z \cdot F} \sinh^{-1} \left(\frac{I}{2 \cdot I_0} \right) \\ &= A \cdot \sinh^{-1} \left(\frac{I}{2 \cdot I_0} \right) \end{aligned} \quad (12)$$

where z presents the number of moles of electrons and I_0 denotes the density of the exchange current, which can be expressed as:

$$I_0 = k_1 \cdot T \cdot e^{-\frac{k_2}{T}} \quad (13)$$

where k_1 and k_2 are empirical constants that express the apparent exchange current.

The concentration voltage loss can be expressed as follows:

$$\begin{aligned} U_{cons} &= \frac{R \cdot T}{z \cdot F} \ln \left(1 - \frac{I}{I_{max}} \right) \\ &= B \cdot \ln \left(1 - \frac{I}{I_{max}} \right) \end{aligned} \quad (14)$$

$$I_{max} = k_3 \frac{\ln(1 - C_{re})}{T} \quad (15)$$

where C_{re} expresses the reactant concentration and k_3 is a constant indicating the limiting current density factor.

The ohmic voltage formula is a function of its internal resistance (R_{int}), which can be presented as follows:

$$U_{ohm} = R_{int} \cdot I = \gamma e^{\delta(298^{-1} - T^{-1})} \quad (16)$$

where γ and δ are constants.

For a fuel cell stack with multiple cells, the output voltage can be expressed as follows:

$$U_{FC} = N_{cells} \cdot U_{FC,cell} = N_{cells} (U_{oc} - U_{act} - U_{cons} - U_{ohm}) \quad (17)$$

where N_{cells} express the number of cells; the operating diagram of the SOFC can be presented in Figure 5.

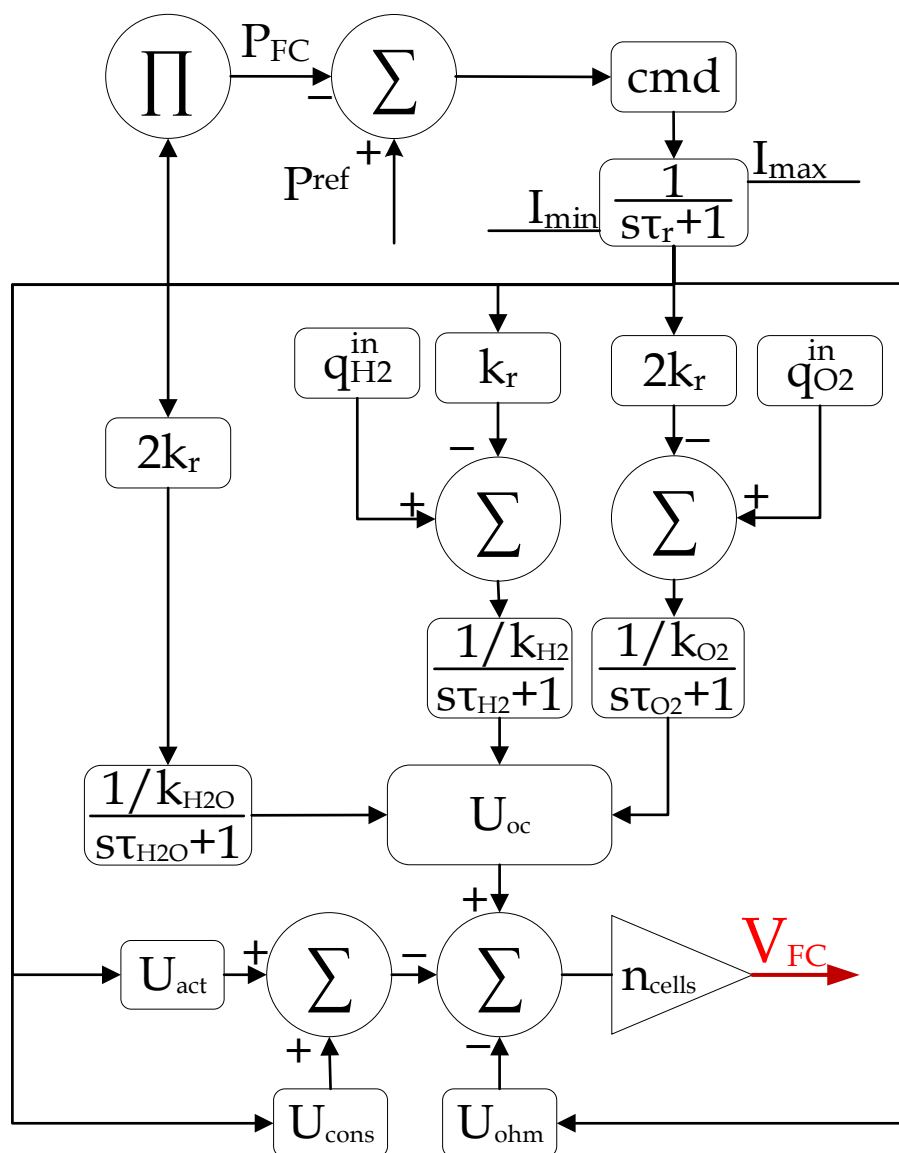


Figure 5. SOFC equivalent circuit.

3. Energy Management Strategy

Electricity efficiency is critical for environmental, economic, and for technological applications. As a result, developing MG energy management is critical, according to [24]. Over the last two decades, the design of energy management systems (EMSs) has piqued the interest of the energy research community. This interest arises from the ongoing and improved development of renewable energy systems and the optimization of EMS technology employing sophisticated energy storage systems, according to [25].

Commercial buildings consume a large quantity of energy; thus, a robust energy management system (EMS) is essential. The EMS has a considerable impact on the system’s overall performance. For the investigated system, the net power (ΔP) is the demanded power by the load that is not provided by solar power. The fuel cell and batteries will be operated under the EMS command to provide net power. The EMS must run the battery within the authorized SoC range to prevent overcharge and deep discharge.

$$\Delta P = P_{Load} - P_{PV} \tag{18}$$

On the other hand, the FC dynamics must be restricted to prevent reactant starvation. Figure 6 depicts the global EMS system where the EMS receives system state data from the acquisition system. The control signals are generated based on these data.

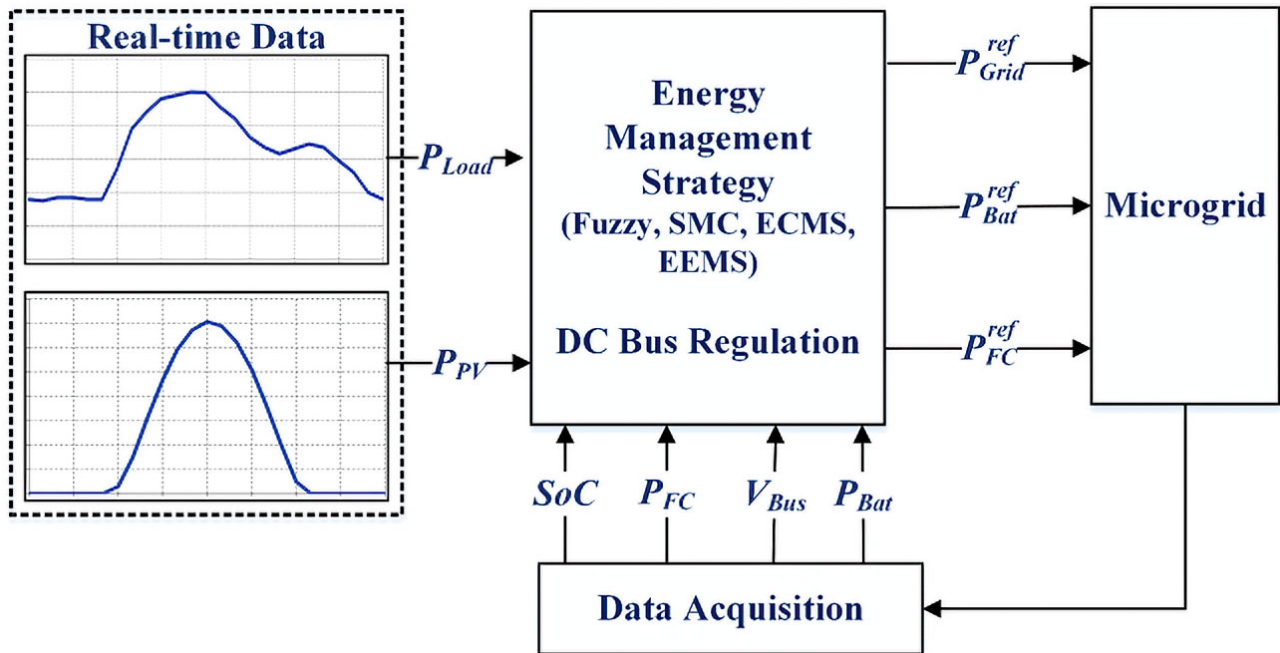


Figure 6. An illustration of the global EMS scheme.

3.1. Fuzzy-Based EMS

The first investigated EMS relies on the fuzzy logic approach to obtain the desired results. The PV generator operates in MPPT mode in this study, and the FC system and battery power are regulated by the generated references, using the fuzzy inference system (FIS)-based EMS. The load power, PV power, and battery SoC are the control inputs, while the outputs are the FC power reference, battery power reference, and utility grid power reference.

Sugeno-type FIS is utilized. The membership functions are shown in Figures 7 and 8, the output surface for the fuzzy inference system is shown in Figure 9, and the fuzzy roles are shown in Table 2.

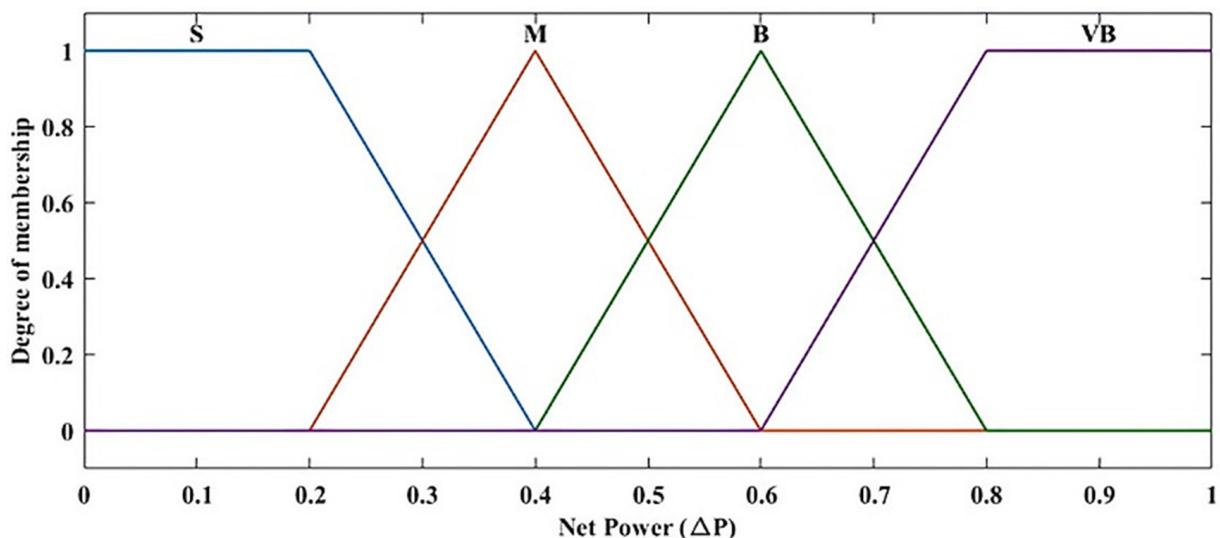


Figure 7. Membership functions for the first input (net power).

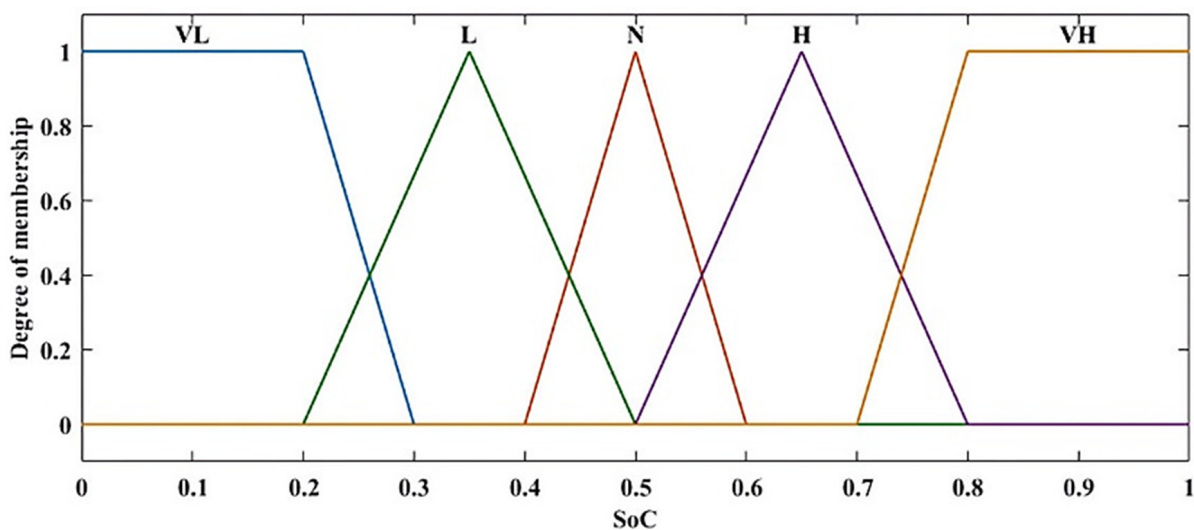


Figure 8. Membership functions for the second input (SoC).

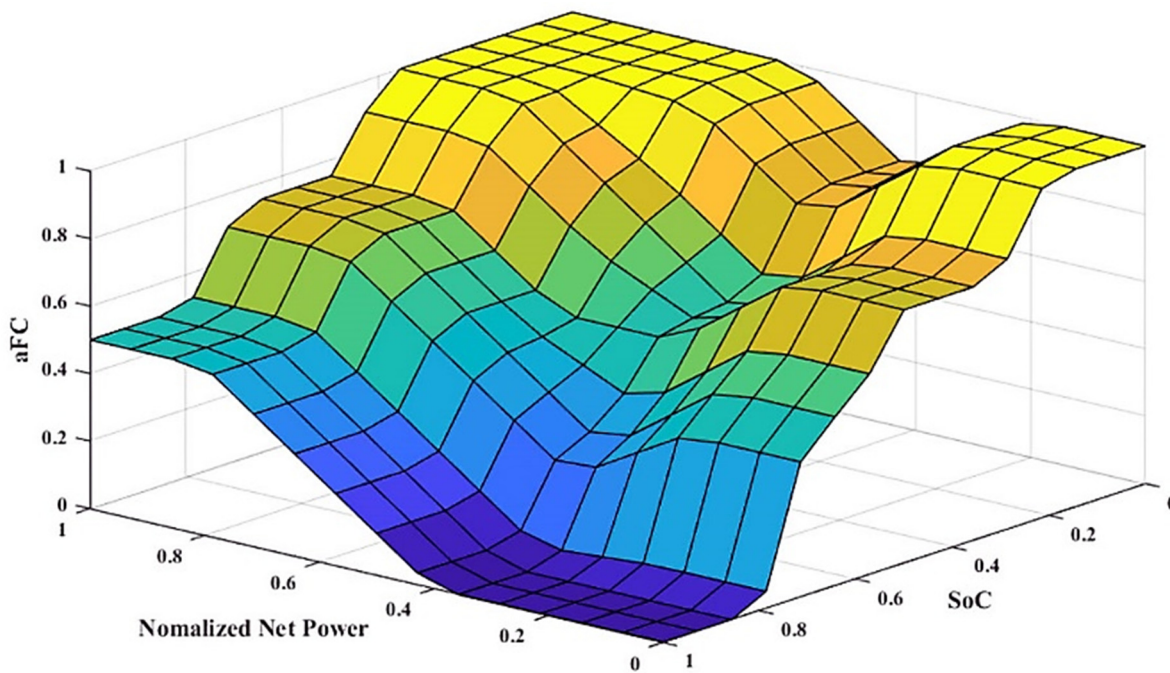


Figure 9. The output surface for the fuzzy inference system.

Table 2. Fuzzy engine roles.

		SoC					
		Very low (VL)	Low (L)	Nature (N)	High (H)	Very high (VH)	Off = 0
ΔP	Small (V)	Max	High	Medium	Low	Off	Low = 0.25
	Medium (M)	Max	High	Medium	Low	Off	Medium = 0.5
	Big (B)	Max	High	Medium	Medium	Low	High = 0.75
	Very big (VB)	Max	Max	High	High	Medium	Max = 1

The current dynamics are limited by using a first-order filter as:

$$I_{FC}^{ref} = \frac{1}{\tau_{FC} \cdot s + 1} \frac{P_{FC}^{ref}}{V_{FC}} \text{ where } I_{FC}^{ref} \in [0, I_{FC}^{max}] \quad (19)$$

where τ_{FC} has to be equivalent to or greater than the FC response constant time.

The battery power is generated using a PI controller to stabilize the DC bus voltage, whereas the grid power is generated based on Equation (28).

3.2. Equivalent Consumption Minimization Strategy

The ECMS seeks to reduce fuel use while keeping the battery SOC within allowable limits. The performance of the ECMS is dependent on the accuracy of the empirical computation of the related fuel consumption, as reported in [26]. The associated goal function is to reduce:

$$P_{Batt}^{opt} = \min(C_{FC} + \beta \cdot C_{Batt}) \quad (20)$$

$$\beta = 1 - 2 \cdot \mu \frac{SoC - 0.5(SoC_{min} + SoC_{max})}{SoC_{min} + SoC_{max}} \quad (21)$$

where C_{Batt} expresses the battery fuel consumption according to the provided energy; μ is a constant (0.6). This equation is subjected to:

$$\begin{aligned} SoC_{min} &\leq SoC \leq SoC_{max} \\ V_{bus}^{min} &\leq V_{bus} \leq V_{bus}^{max} \\ P_{FC}^{min} &\leq P_{FC} \leq P_{FC}^{max} \end{aligned} \quad (22)$$

The FC output power can be calculated as follows:

$$P_{FC}^{ref} = \Delta P - P_{Grid}^{ref} - P_{Batt}^{opt} \quad (23)$$

The ECMS scheme is illustrated in Figure 10.

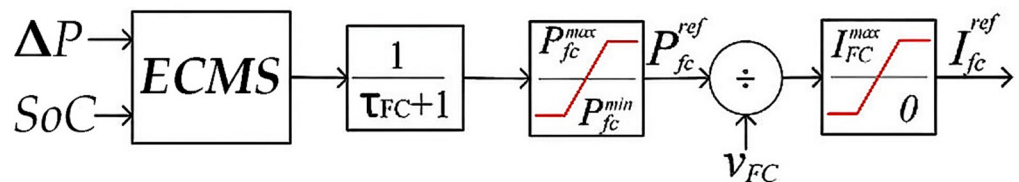


Figure 10. The generation of FC power reference using ECMS.

3.3. External Energy Maximization Strategy

The primary goal of this strategy is to supply the least amount of fuel possible while respecting the battery and DC bus capacitor power limits [27]. Its objective function is to maximize the energy provided by the battery and the bus capacitor, as follows:

$$P_{Batt}^{opt} = \min(\Delta T \cdot P_{Batt} + 0.5 \cdot C_{bus} \cdot (\Delta v)^2) \quad (24)$$

where ΔT represents the sampling time, and Δv represents the charge/discharge voltage. This equation is subjected to:

$$\begin{aligned} P_{Batt} &\leq (SoC - SoC_{min}) V_{Batt} \cdot Q_{Batt} \\ V_{bus}^{min} - V_{bus} &\leq \Delta v \leq V_{bus}^{max} - V_{bus} \\ P_{Batt}^{charge} &\leq P_{Batt} \leq P_{Batt}^{discharge} \end{aligned} \quad (25)$$

where V_{batt} and Q_{batt} are the battery nominal voltage and capacity; the operating scheme of the EEMS is given in Figure 11. In contrast to Figure 10, the inputs in Figure 11 are the net power and the bus voltage, where the used algorithm is EEMS.

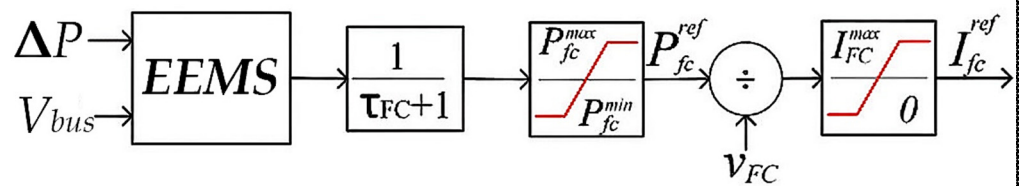


Figure 11. The generation of FC power reference using EEMS.

3.4. State Machine Control

State Machine Control is a strategy based on switching rules [28]. Its principle is to select the operating state according to the inputs: ΔP and battery SOC. According to the state of its inputs, it charges or discharges the battery, as explained in Figure 12.

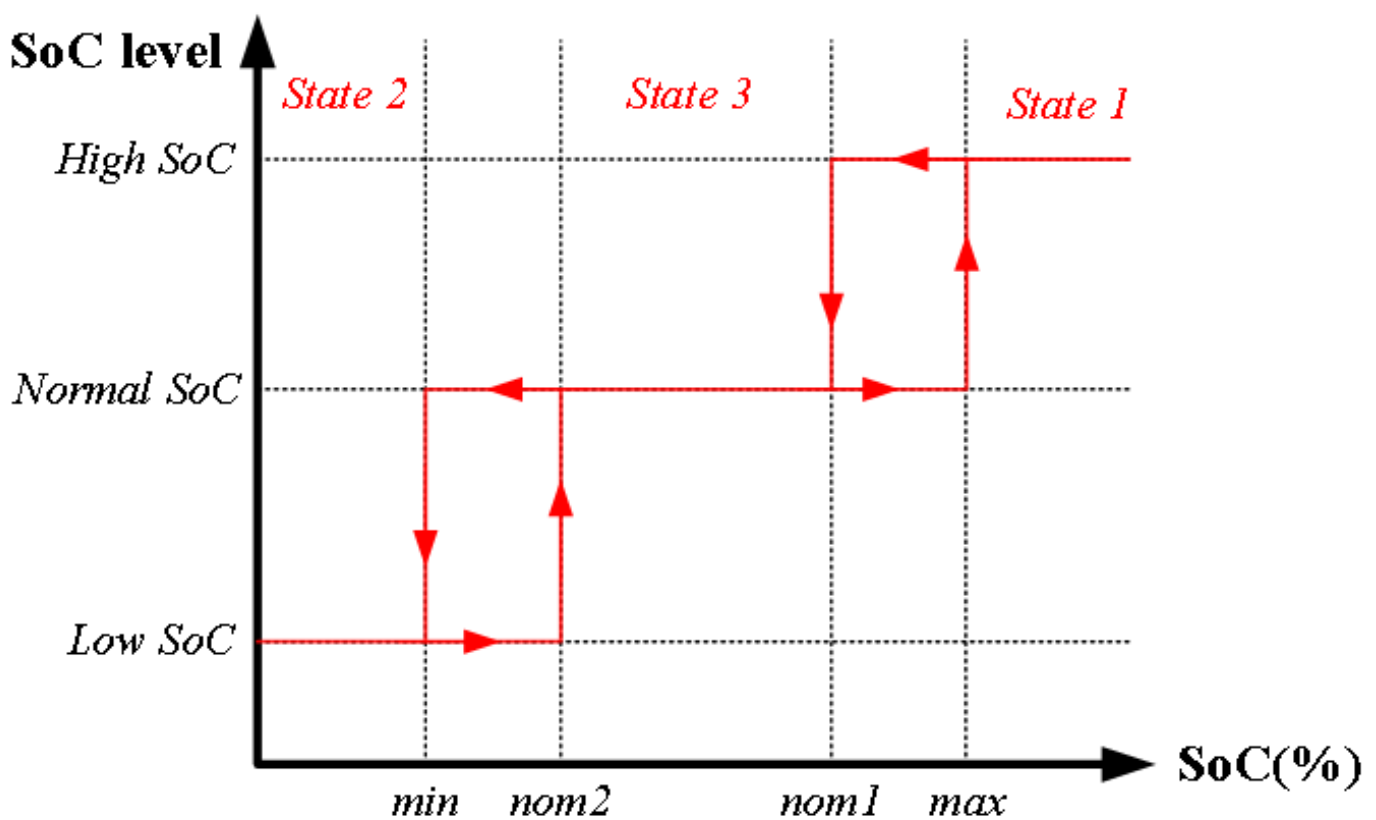


Figure 12. Illustration of the SMC control scheme states.

3.5. Grid Power Reference Generation

The microgrid will turn into (on-grid) mode if the battery SoC exceeds its allowable limits by injecting or absorbing the power from the common line. Its power reference is given as:

$$P_{Grid}^{ref} = \Delta P - P_{Batt}^{req} - P_{FC} \tag{26}$$

where P_{Batt}^{req} is the required power by the battery to maintain its SoC, which can be calculated as follows:

$$P_{Batt}^{req} = k_{grid} \cdot V_{Batt} \cdot Q_{Batt} \tag{27}$$

where k_{grid} is again generated by a state machine controller. Its value depends on the batter's SoC, and its base roles are given as Algorithm 1:

Algorithm 1 Utility grid connection roles

```

1   if SoC < SoCmin do
2   if ΔP − PFCmax do
3   PGridref = ΔP − PFC + (SoCmin − SoC)QBatt·VBatt
4   else
5   PGridref = (SoCmin − SoC)QBatt·VBatt
6   end
7   elseif SoC > SoCmax and ΔP < 0 do
8   PGridref = ΔP
9   elseif SoC < SoCmax and SoC > SoCmin do
10  PGridref = 0
11  end

```

The inverter dynamics have to be limited to protect the battery from the overcurrent charge and to restrict the voltage from the high overshoot as follows:

$$I_{Gid}^{ref} = \frac{1}{\tau_{grid} \cdot s + 1} \frac{P_{Grid}^{ref}}{V_{Bus}} \quad (28)$$

where τ_{grid} is the constant time of the inverter, the operation of the grid inverter is illustrated in Figure 13.

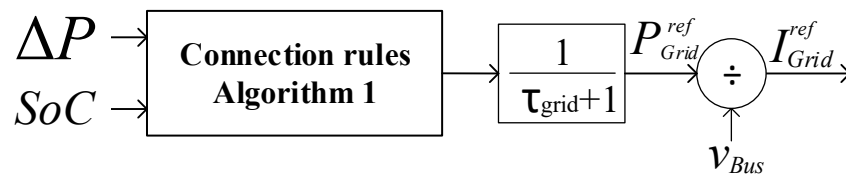


Figure 13. Grid connector block scheme.

3.6. DC Bus Stabilization

The principal role of the battery is to stabilize the DC bus voltage by regulating the power in the commune line. In this study, a PI controller is employed to generate the reference DC bus power, which ensures a stable voltage and satisfies the load power. The dc bus energy E_{bus} can be expressed as [29]:

$$\dot{E}_{Bus} = -\Delta P + P_{FC} + P_{Batt} + P_{Grid} \quad (29)$$

Therefore, the battery power reference can be obtained as a function of the dc bus energy, as:

$$P_{Batt}^{ref} = \dot{E}_{Bus} + \Delta P - P_{FC} - P_{Grid} \quad (30)$$

The bus energy is zero at the steady state. However, its value will typically charge depending on the difference between the reference and the measured voltage. Its value will be generated using a PI controller, which regulates the bus energy as follow:

$$\dot{E}_{Bus} = (E_{Bus}^{ref} - E_{Bus}) \left(k_p + \frac{k_i}{s} \right) \quad (31)$$

$$\begin{aligned} E_{Bus}^{ref} &= 0.5 \cdot V_{Bus}^{ref} \cdot C_{Bus} \\ E_{Bus} &= 0.5 \cdot V_{Bus} \cdot C_{Bus} \end{aligned} \quad (32)$$

where V_{Bus}^{ref} is the bus voltage reference and C_{Bus} is the bus capacitance.

The exchanged power must be limited to protect the battery. The maximum amount of the delivered electrical energy should be between 10 and 20% of its total capacity. Therefore, the reference power can be written as:

$$\left| P_{Batt}^{ref} \right| < V_{Batt} \cdot Q_{Batt} \cdot (0.1 \sim 0.2) \quad (33)$$

The reference current can be written as:

$$I_{Batt}^{ref} = \frac{P_{Batt}^{ref}}{V_{Batt}} \quad (34)$$

The maximum discharge current must be lighter than 10% of the capacity, and the maximum charge current must be smaller than 2%.

$$-0.02 \cdot Q_{Batt} < I_{Batt}^{ref} < 0.1 \cdot Q_{Batt} \quad (35)$$

The bus stabilization control low is illustrated in Figure 14.

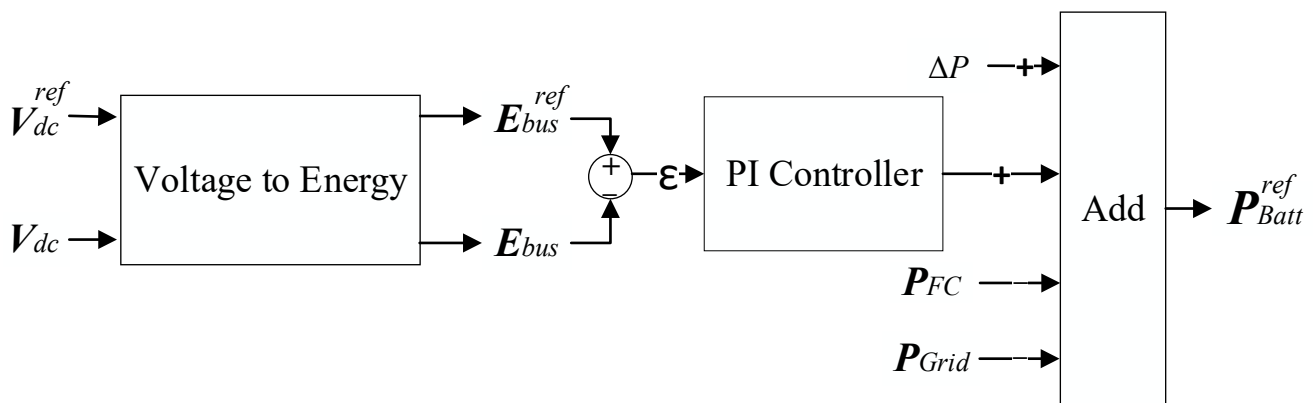


Figure 14. The proposed DC Bus stabilization control scheme.

4. Results and Discussion

The power system parameters are based on those reported in [11]. In the considered building, the DC bus voltage is set at 380 V; the fuel cell maximum power was set at 250 kW. The used battery of 220 V 1500 Ah. Table 3 presents the power system parameters. In this study, the min SoC is supposed to be 30%, whereas the remaining 30% is reserved for the crucial loads in case of a blackout.

Table 3. Power System Parameters.

Parameters	Value	Unit
Bus voltage reference	380	V
Battery capacity	1500	Ah
Battery voltage	220	V
SoC max	90	%
SoC min	30	%
FC max output power	250	kW

To verify the performance of each EMS, a simulation was carried out in the MATLAB/Simulink framework for five days (120 h). In many papers dealing with RTO strategies, the studied load and solar power profiles are 24 h profiles, such as [30,31]. A five day profile is chosen to validate the system performance in real time, where the chosen profile proposes different solar and load behaviors and scenarios to emulate the behavior of

the physical system. The solar irradiance is provided in Figure 15, and the power profiles are provided in Figure 16. In this study, two profiles for the load and the solar power are provided by the House Load toolbox [32]. Generally, these papers take different power profiles to demonstrate the performance of the proposed EMS under different operating conditions. In this paper, a single profile of 120 h has different operating conditions, such as cloudy, partially cloudy, and sunny days; the load behavior also changes to emulate the working and the weekends.

A cloudy profile is operated, so the solar power is very fluctuating. This will affect the battery output power responsible for stabilizing the DC bus voltage. The EMS has to supply the net power, represented in Figure 17.

The delivered power from each source with EEMS-, ECMS-, SMC-, and FLC-based EMS are illustrated in Figures 18–21. The recorded SoC for each strategy is illustrated in Figure 22.

The SoC decreases much faster using ECMS and Fuzzy strategies, meaning the battery shares more power when employing these strategies. The grid power will prevent the battery from overcharging or deep-discharge; however, charging/discharging cycles will reduce the battery lifespan. Furthermore, it raises grid dependency by increasing the demand for utility grid power. It is observed that the EEMS and SMC strategies utilize the FC power more than the battery. The charging/discharging cycles are limited in utilizing the strategies.

As a consequence, an extended battery lifespan is achieved. Although the EEMS are based on the DC bus capacitance, it offers extraordinary efficiency (84.91%). The appropriate choice of the SMC rules will increase its efficiency (84.18%) compared with ECMS (76.27%) and FLC (76.30%).

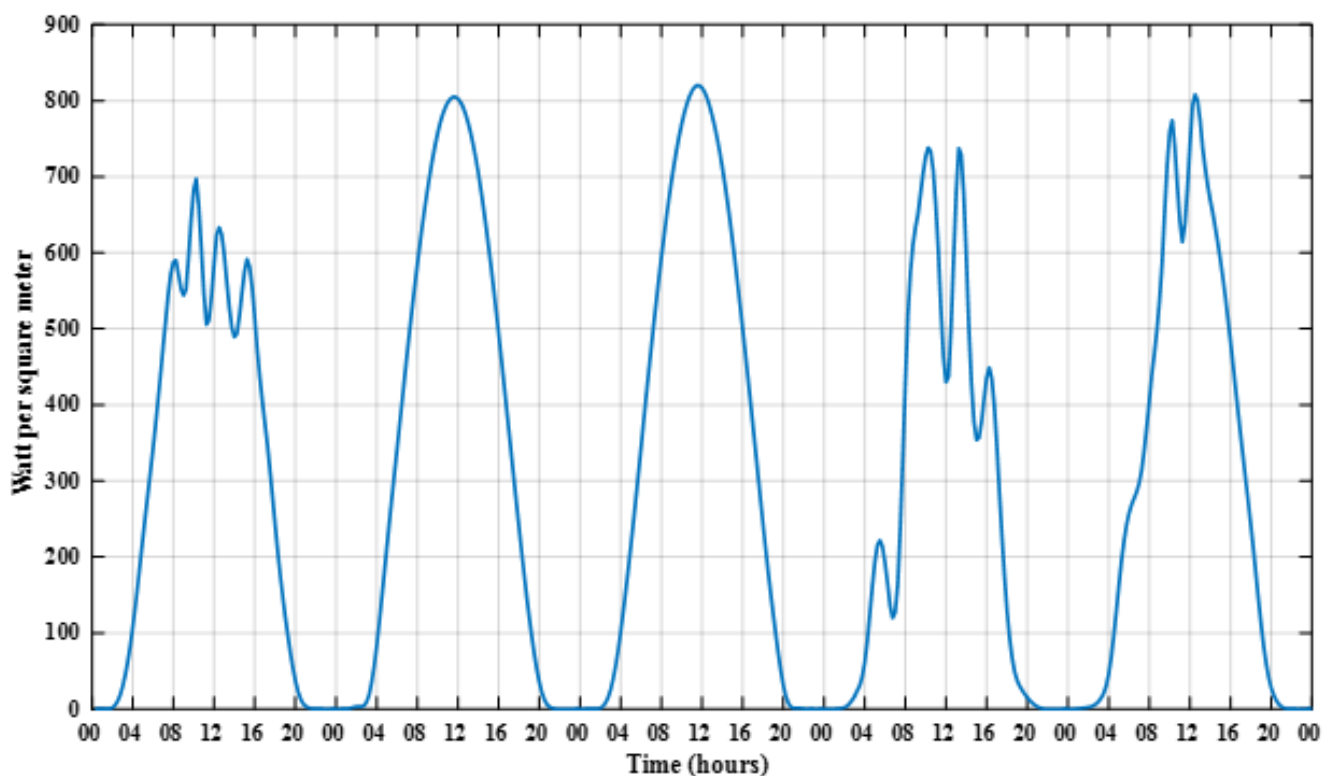


Figure 15. Solar irradiance profile for five days (W/m^2) [32].

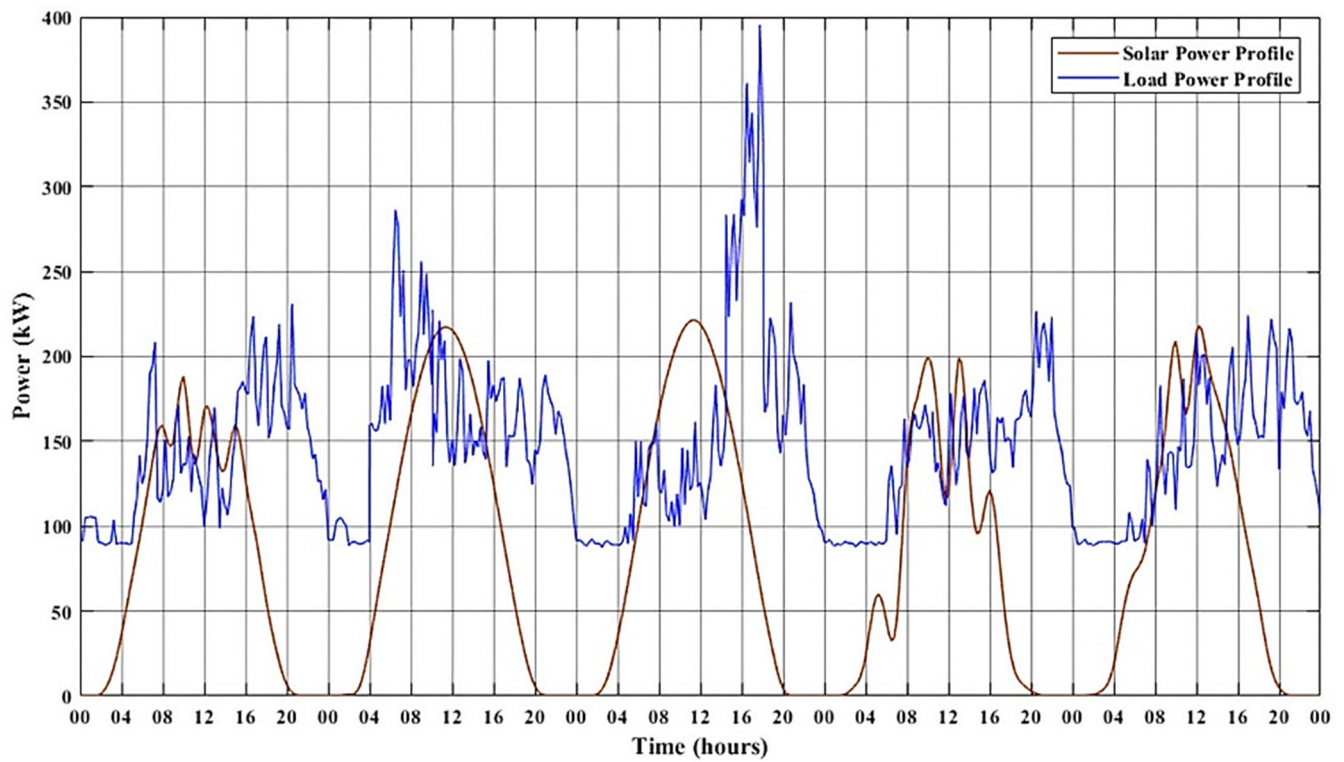


Figure 16. Used load and solar power profiles for five days (kW) [32].

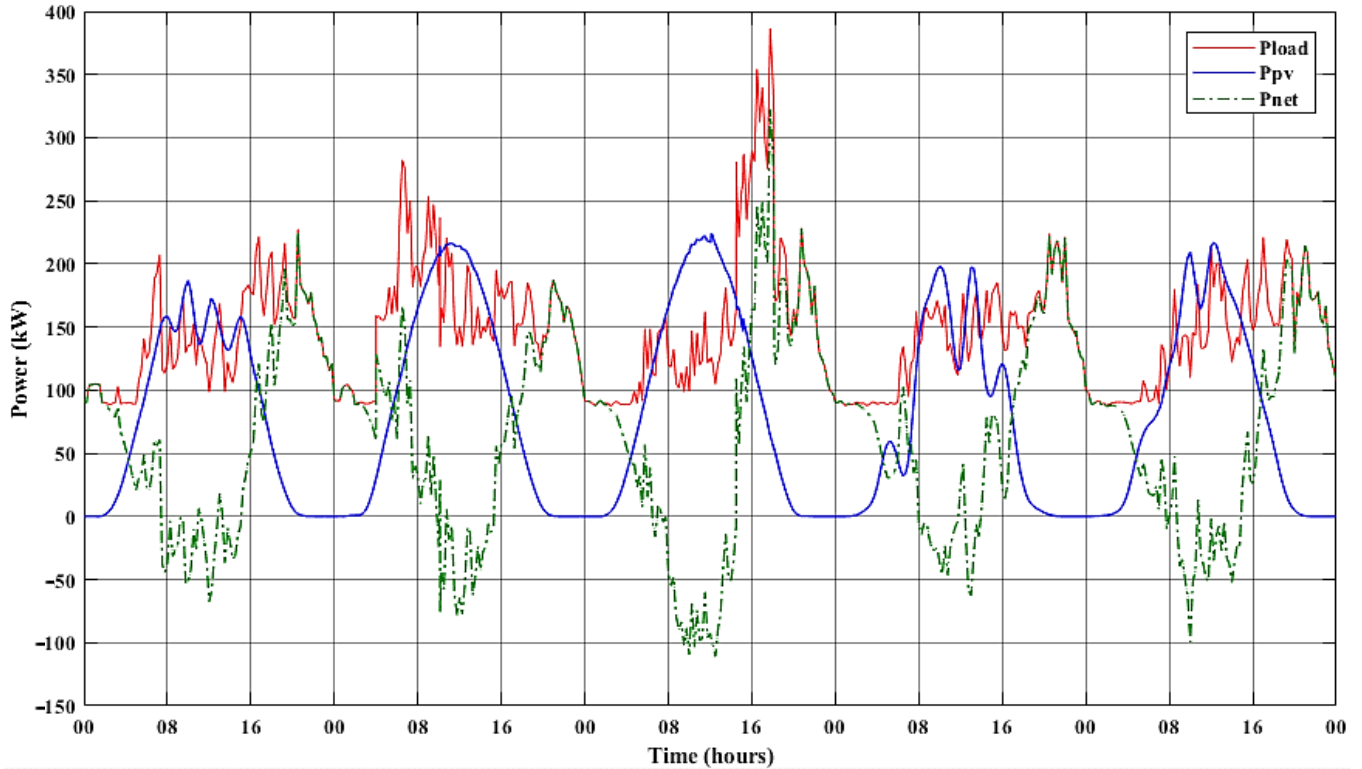


Figure 17. The measured load, the renewable, and the net power (kW).

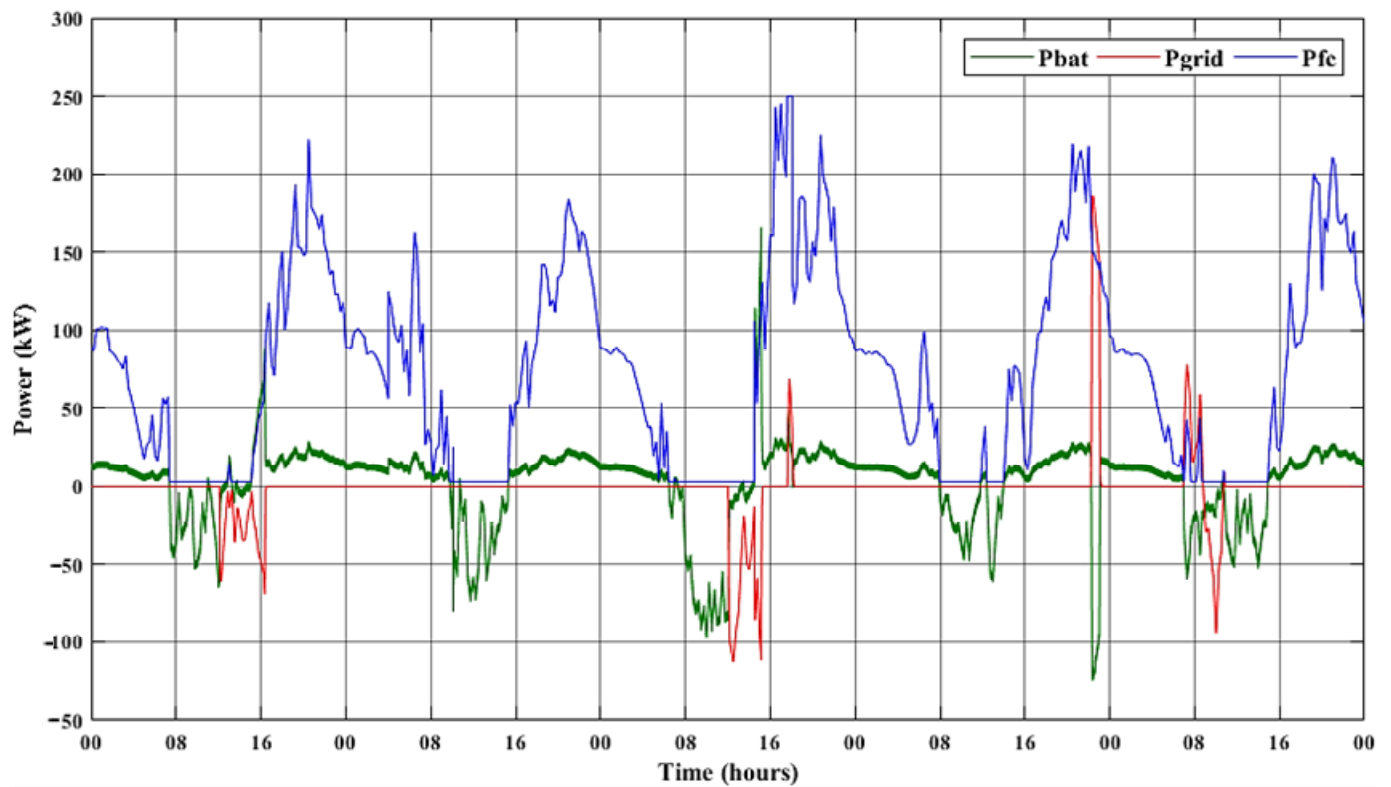


Figure 18. FC, battery, and grid power using EEMS (kW).

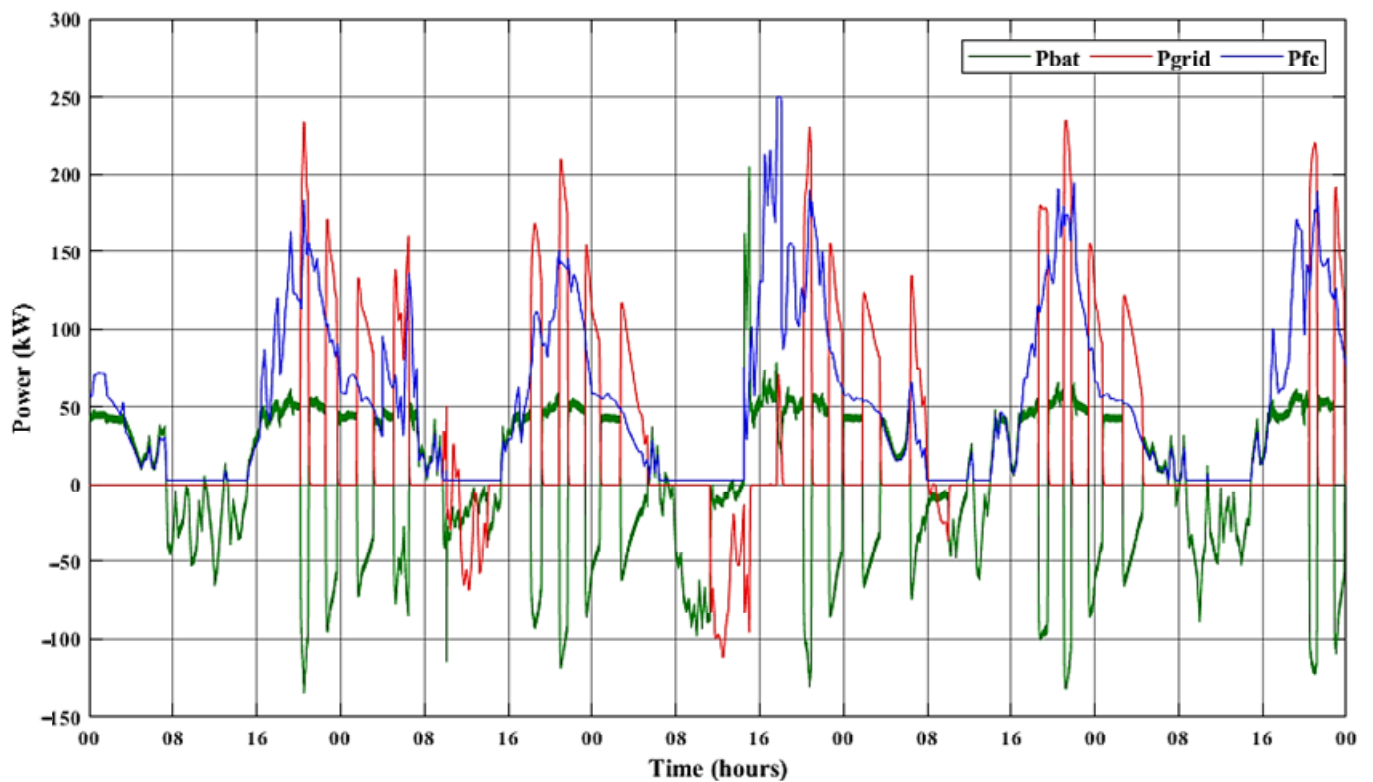


Figure 19. FC, battery, and grid power using ECMS (kW).

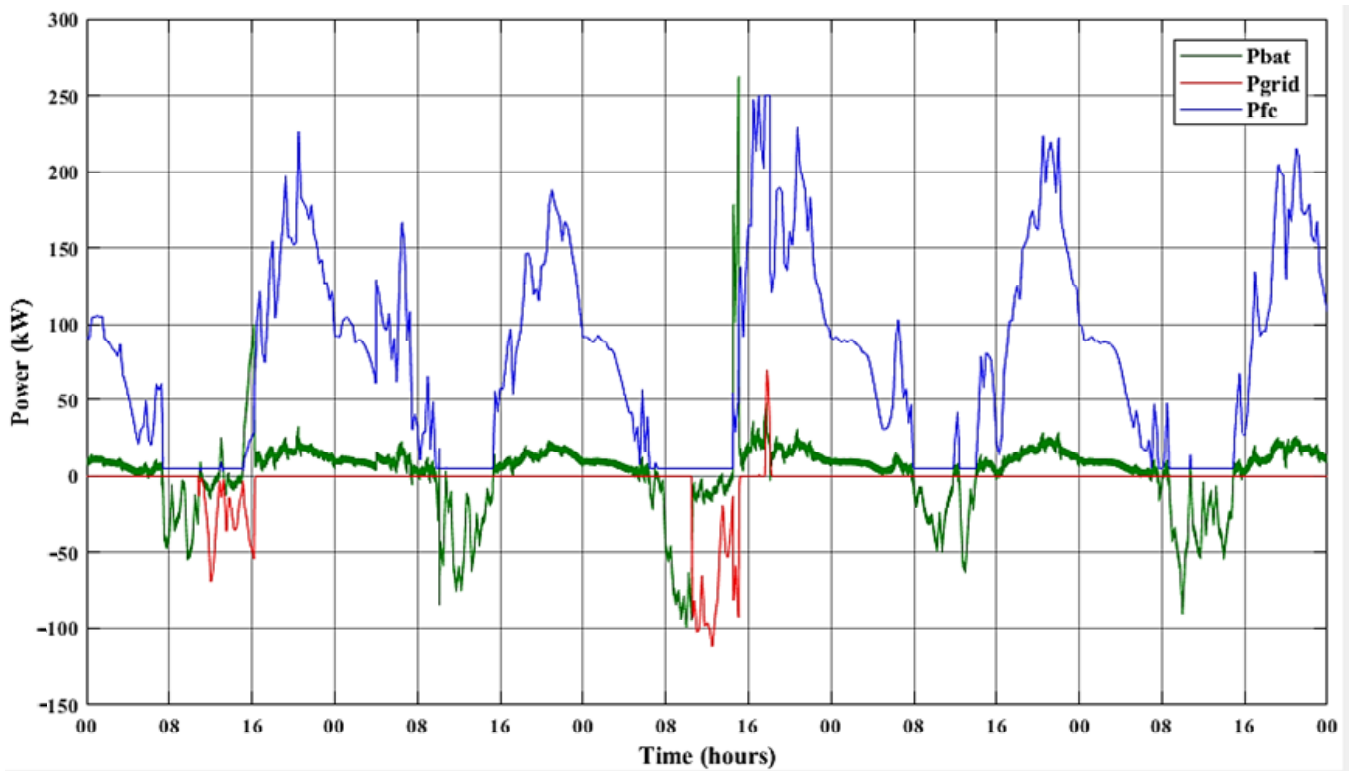


Figure 20. FC, battery, and grid power using SMC (kW).

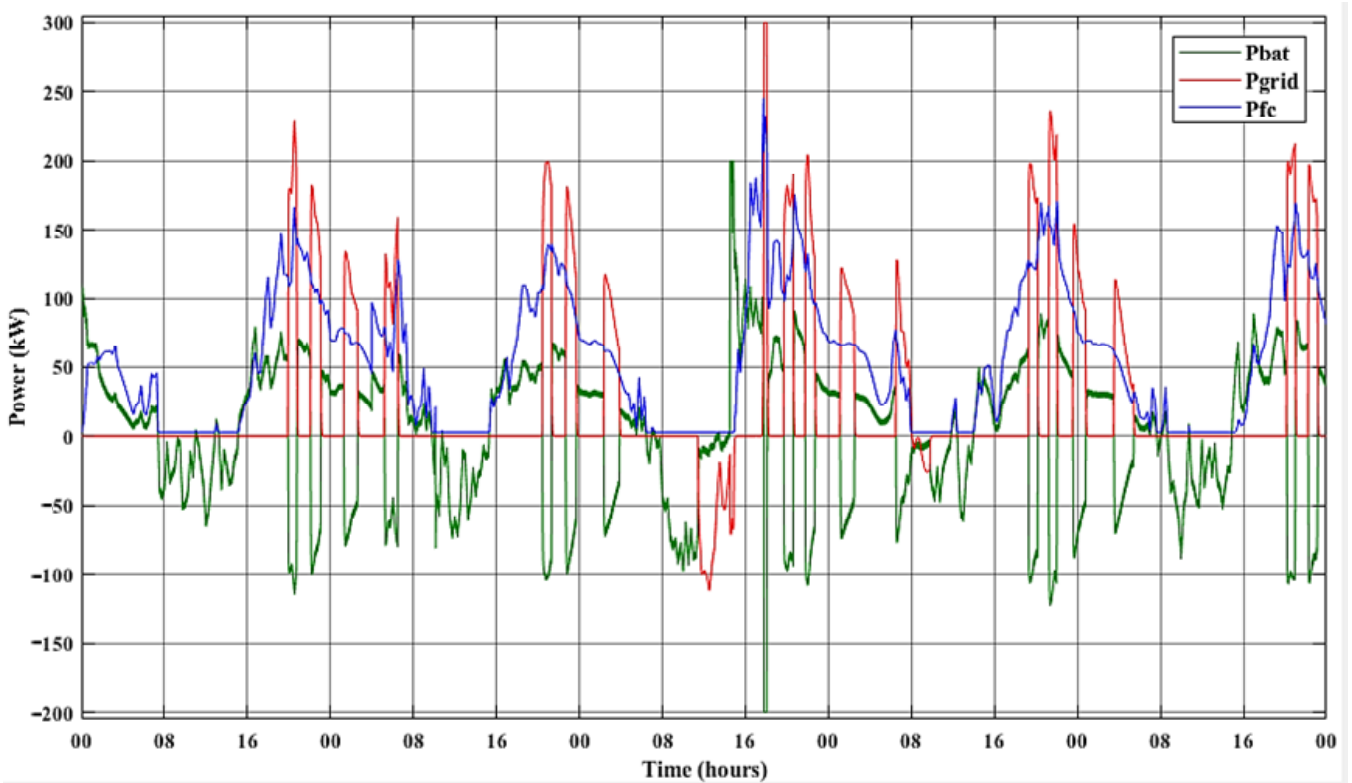


Figure 21. FC, battery, and grid power using FLC-based EMS (kW).

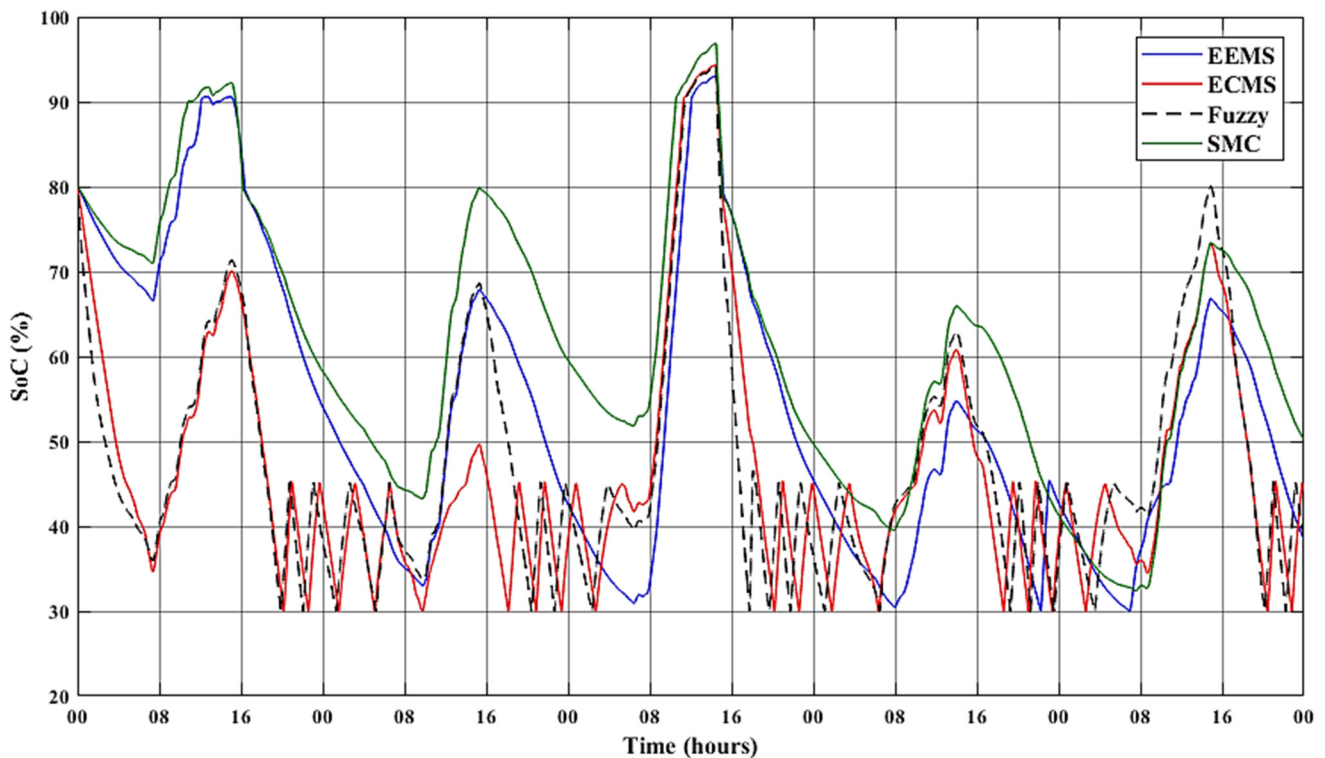


Figure 22. Battery State of Charge (%).

The simulation result statistics are given in Table 4 and Figure 23.

Table 4. Simulation results.

	Efficiency (%)	Final SoC (%)	FC Energy (KWh)	Grid Energy (KWh)	Paid Energy (KWh)	Power Saving (%)
EEMS	84.91	38.46	83,712	−1826	81,886	6.11
ECMS	76.27	44.15	62,070	24,199	86,270	1.83
SMC	80.18	50.20	87,175	−4380	82,794	5.07
Fuzzy	76.30	38.55	62,865	24,349	87,215	NA

The results illustrated above prove the superiority of the EEMS as a suitable strategy for commercial buildings in terms of electrical efficiency (84.91%), power saving (6.11%), and paid energy (81,886).

As mentioned before, each strategy controls the battery power. Accordingly, the strategy performance will directly affect the DC bus voltage. Figure 24 shows the obtained DC bus voltage of each strategy. The measurement statistics are given in Table 5 and Figure 25. Although these results show a relatively small static error (2 V), the EEMS ensures excellent power quality. As a result of the low standard deviation (std) provided by the EEMS, the latter will prevent the FC system and the battery from premature aging.

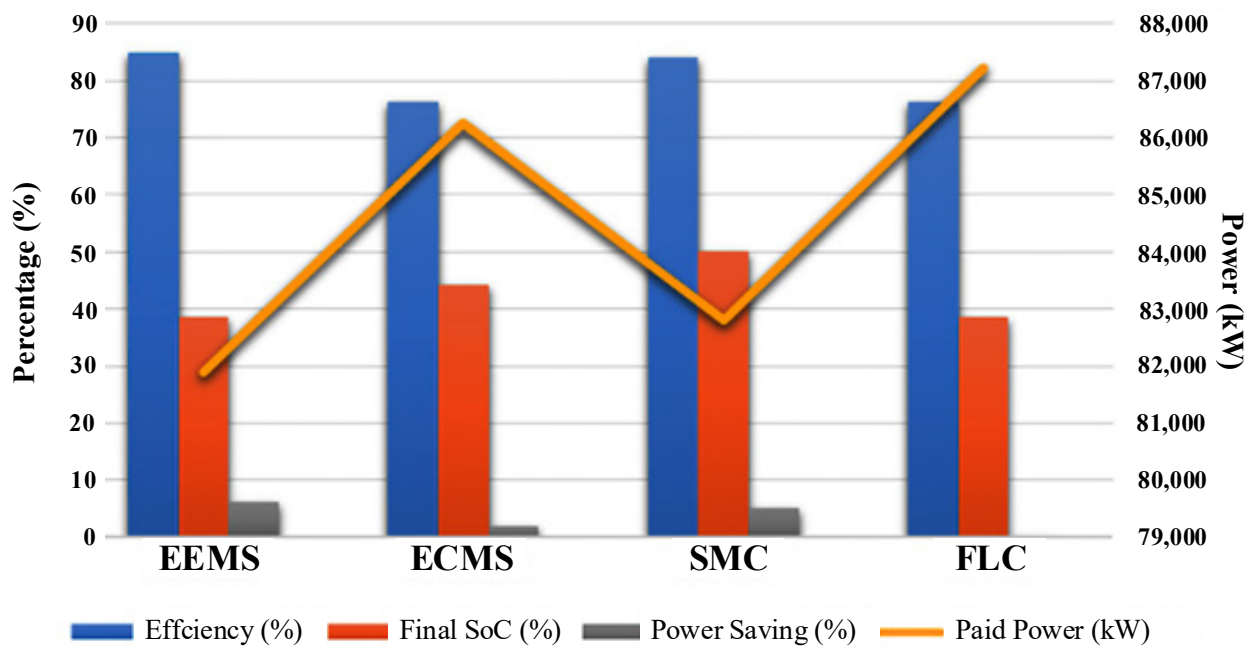


Figure 23. Simulation Statistics.

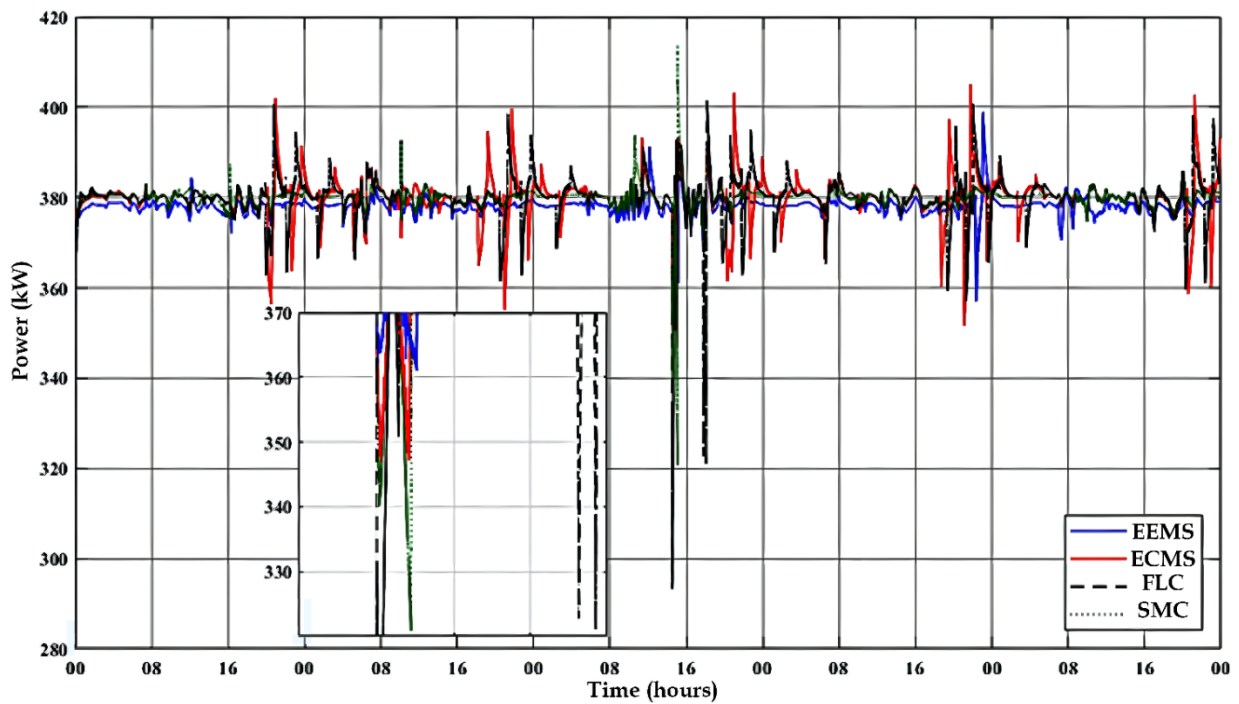


Figure 24. DC bus voltage (V).

Table 5. Bus voltage statistics.

	Min	Max	Mean	Median	Range	StD
EEMS	357	398.9	378	378.2	41.95	2.07
ECMS	346.9	405	380	380.3	58.12	4.59
SMC	320	413	380	380.2	93.16	2.54
Fuzzy	293.3	401	380	380.3	108.1	4.88

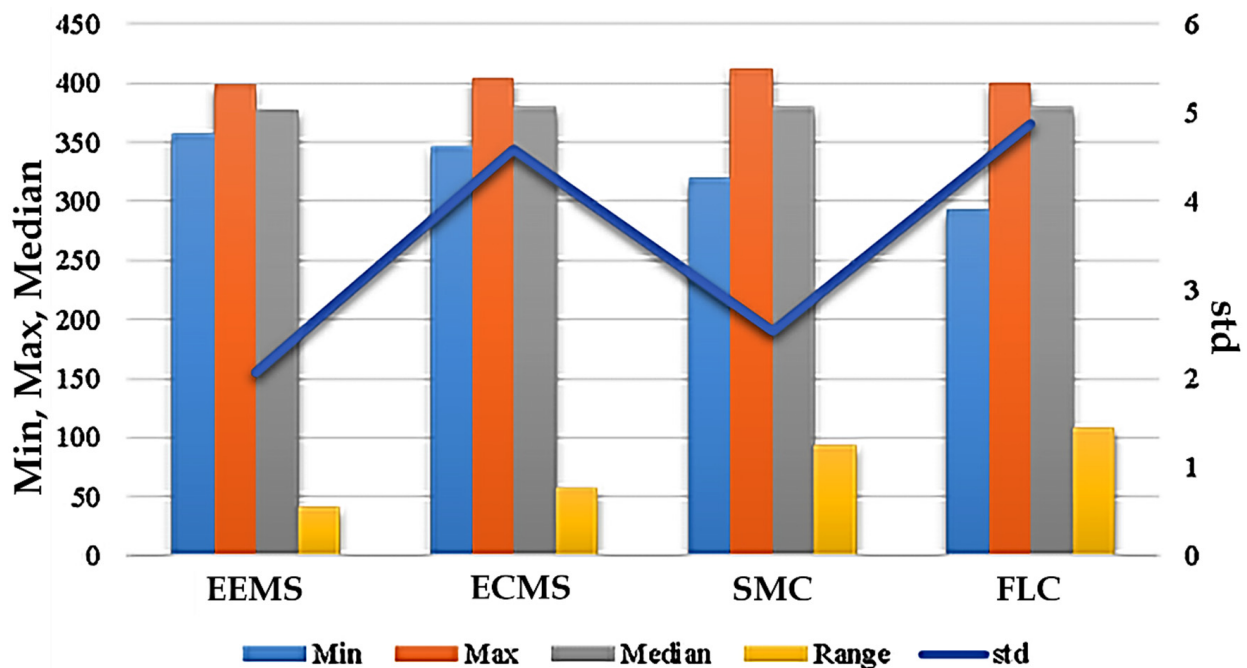


Figure 25. Bus voltage graphical statistics.

5. Conclusions

A comprehensive comparison of four energy management strategies is accomplished. These strategies include fuzzy logic control (FLC), equivalent consumption minimization strategy (ECMS), external energy maximization strategy (EEMS), and state machine control (SMC). These strategies are adopted to achieve optimal performance against severe load and solar power fluctuations. The fundamental comparison indicators are overall system efficiency, power-saving, and the final SoC. The obtained results prove that EEMS provides optimal performance. It operates the system with an efficiency of 84.91% and a power-saving of 6.11%. This strategy can also ensure the power quality for the building and improve the lifespan of the power sources. The system can utilize battery safety with the most extended possible lifespan using the EEMS and SMC (low charging/discharging cycles). In addition, the limited voltage provided by EEMS (41.95 V) gives the battery more safety. The reduced bus voltage (StD 2.068) ensures safe operation for the FC. Eventually, and from the previous analysis, the EEMS provides the most satisfactory performance compared to the other strategies. The results obtained showed that the EEMS performed better than the other studied strategies. However, optimized versions of these strategies may provide a superior performance, such as adaptive optimal fuzzy or salp swarm algorithm (SSA)-based EEMS, and so on. The performance of these strategies will be investigated in future works.

Author Contributions: Conceptualization, H.R., S.F. and A.F.; Methodology, S.F. and A.F.; Software, S.F.; Formal analysis, H.R. and S.F.; Writing—original draft, H.R., R.M.G., S.F., A.F., M.M.G. and R.A.; Writing—review & editing, H.R., R.M.G., S.F., A.F., M.M.G. and R.A.; Project administration, H.R. and R.M.G. All authors have read and agreed to the published version of the manuscript.

Funding: This work was funded by the Deanship of Scientific Research at Princess Nourah bint Abdulrahman University, through the Research Groups Program Grant no. (RGP-1443-0046).

Institutional Review Board Statement: Not applicable.

Informed Consent Statement: Not applicable.

Data Availability Statement: Not applicable.

Conflicts of Interest: The authors declare no conflict of interest.

References

1. Wang, F.; Xie, J.; Wu, S.; Li, J.; Barbieri, D.M.; Zhang, L. Life cycle energy consumption by roads and associated interpretative analysis of sustainable policies. *Renew. Sustain. Energy Rev.* **2021**, *141*, 110823. [[CrossRef](#)]
2. Gui, E.M.; Diesendorf, M.; MacGill, I. Distributed energy infrastructure paradigm: Community microgrids in a new institutional economics context. *Renew. Sustain. Energy Rev.* **2017**, *72*, 1355–1365. [[CrossRef](#)]
3. Mohabat Doost, D.; Buffa, A.; Brunetta, G.; Salata, S.; Mutani, G. Mainstreaming Energetic Resilience by Morphological Assessment in Ordinary Land Use Planning. The Case Study of Moncalieri, Turin (Italy). *Sustainability* **2020**, *12*, 4443. [[CrossRef](#)]
4. Ehigiamusoe, K.U.; Dogan, E. The role of interaction effect between renewable energy consumption and real income in carbon emissions: Evidence from low-income countries. *Renew. Sustain. Energy Rev.* **2022**, *154*, 111883. [[CrossRef](#)]
5. Srivastava, C.; Tripathy, M. DC microgrid protection issues and schemes: A critical review. *Renew. Sustain. Energy Rev.* **2021**, *151*, 111546. [[CrossRef](#)]
6. Mirsaedi, S.; Dong, X.; Said, D.M. Towards hybrid AC/DC microgrids: Critical analysis and classification of protection strategies. *Renew. Sustain. Energy Rev.* **2018**, *90*, 97–103. [[CrossRef](#)]
7. Majeed Butt, O.; Zulqarnain, M.; Majeed Butt, T. Recent advancement in smart grid technology: Future prospects in the electrical power network. *Ain. Shams. Eng. J.* **2021**, *12*, 687–695. [[CrossRef](#)]
8. Dagar, A.; Gupta, P.; Niranjana, V. Microgrid protection: A comprehensive review. *Renew. Sustain. Energy Rev.* **2021**, *149*, 111401. [[CrossRef](#)]
9. Sandelic, M.; Peyghami, S.; Sangwongwanich, A.; Blaabjerg, F. Reliability aspects in microgrid design and planning: Status and power electronics-induced challenges. *Renew. Sustain. Energy Rev.* **2022**, *159*, 112127. [[CrossRef](#)]
10. Ferahtia, S.; Djeroui, A.; Rezk, H.; Houari, A.; Zeghlache, S.; Machmoum, M. Optimal control and implementation of energy management strategy for a DC microgrid. *Energy* **2022**, *238*, 121777. [[CrossRef](#)]
11. Ferahtia, S.; Rezk, H.; Abdelkareem, M.A.; Olabi, A.G. Optimal techno-economic energy management strategy for building's microgrids based on bald eagle search optimization algorithm. *Appl. Energy* **2022**, *306*, 118069. [[CrossRef](#)]
12. Fathy, A.; Ferahtia, S.; Rezk, H.; Yousri, D.; Abdelkareem, M.A.; Olabi, A.G. Optimal adaptive fuzzy management strategy for fuel cell-based DC microgrid. *Energy* **2022**, *247*, 123447. [[CrossRef](#)]
13. Vossos, V.; Gerber, D.; Bennani, Y.; Brown, R.; Marnay, C. Techno-economic analysis of DC power distribution in commercial buildings. *Appl. Energy* **2018**, *230*, 663–678. [[CrossRef](#)]
14. AlLee, G.; Tschudi, W. Edison Redux: 380 Vdc Brings Reliability and Efficiency to Sustainable Data Centers. *IEEE Power Energy Mag.* **2012**, *10*, 50–59. [[CrossRef](#)]
15. Huang, J.; Fan, J.; Furbo, S.; Chen, D.; Dai, Y.; Kong, W. Economic analysis and optimization of household solar heating technologies and systems. *Sustain. Energy Technol. Assess.* **2019**, *36*, 100532. [[CrossRef](#)]
16. Hidalgo León, R.; Almeida Pazmiño, G.; Jácome Ruiz, P.; Soriano Idrovo, G.; Urquiza Guevara, J. A Survey on Technologies to Implement Battery Emulators based on DC/DC Power Converters. In Proceedings of the 14th Latin American and Caribbean Conference for Engineering and Technology, San Jose, Costa Rica, 20–22 July 2016. [[CrossRef](#)]
17. He, H.; Xiong, R.; Fan, J. Evaluation of Lithium-Ion Battery Equivalent Circuit Models for State of Charge Estimation by an Experimental Approach. *Energies* **2011**, *4*, 582–598. [[CrossRef](#)]
18. US Department of Energy. *Comparison of Fuel Cell Technologies; Energy Efficiency & Renewable Energy*: Washington, DC, USA, 2016.
19. Wang, C.; Nehrir, M.H.H. A Physically Based Dynamic Model for Solid Oxide Fuel Cells. *IEEE Trans. Energy Convers.* **2007**, *22*, 887–897. [[CrossRef](#)]
20. Belila, A.; Amirat, Y.; Benbouzid, M.; Berkouk, E.M.; Yao, G. Virtual synchronous generators for voltage synchronization of a hybrid PV-diesel power system. *Int. J. Electr. Power Energy Syst.* **2020**, *117*, 105677. [[CrossRef](#)]
21. Wang, N.; Wang, D.; Xing, Y.; Shao, L.; Afzal, S. Application of co-evolution RNA genetic algorithm for obtaining optimal parameters of SOFC model. *Renew. Energy* **2020**, *150*, 221–233. [[CrossRef](#)]
22. Chakraborty, U. Reversible and Irreversible Potentials and an Inaccuracy in Popular Models in the Fuel Cell Literature. *Energies* **2018**, *11*, 1851. [[CrossRef](#)]
23. Chakraborty, S.; Simões, M.G.; Kramer, W.E. (Eds.) *Power Electronics for Renewable and Distributed Energy Systems*; Springer: London, UK, 2013. [[CrossRef](#)]
24. Jiang, Q.; Xue, M.; Geng, G. Energy management of microgrid in grid-connected and stand-alone modes. *IEEE Trans. Power Syst.* **2013**, *28*, 3380–3389. [[CrossRef](#)]
25. Vásquez, L.O.P.; Ramírez, V.M.; Thanapalan, K. A Comparison of Energy Management System for a DC Microgrid. *Appl. Sci.* **2020**, *10*, 1071. [[CrossRef](#)]
26. Motapon, S.N.; Dessaint, L.-A.; Al-Haddad, K. A Robust H₂-Consumption-Minimization-Based Energy Management Strategy for a Fuel Cell Hybrid Emergency Power System of More Electric Aircraft. *IEEE Trans. Ind. Electron.* **2014**, *61*, 6148–6156. [[CrossRef](#)]
27. Ahmadi, S.; Bathaee, S.M.T.; Hosseinpour, A.H. Improving fuel economy and performance of a fuel-cell hybrid electric vehicle (fuel-cell, battery, and ultra-capacitor) using optimized energy management strategy. *Energy Convers. Manag.* **2018**, *160*, 74–84. [[CrossRef](#)]

28. Han, Y.; Yang, H.; Li, Q.; Chen, W.; Zare, F.; Guerrero, J.M. Mode-triggered droop method for the decentralized energy management of an islanded hybrid PV/hydrogen/battery DC microgrid. *Energy* **2020**, *199*, 117441. [[CrossRef](#)]
29. Ferahtia, S.; Djerioui, A.; Zeghlache, S.; Houari, A. A hybrid power system based on fuel cell, photovoltaic source and supercapacitor. *SN Appl. Sci.* **2020**, *2*, 940. [[CrossRef](#)]
30. Liu, N.; Chen, Q.; Liu, J.; Lu, X.; Li, P.; Lei, J.; Zhang, J. A Heuristic Operation Strategy for Commercial Building Microgrids Containing EVs and PV System. *IEEE Trans. Ind. Electron.* **2015**, *62*, 2560–2570. [[CrossRef](#)]
31. Al-Sakkaf, S.; Kassas, M.; Khalid, M.; Abido, M.A. An energy management system for residential autonomous DC microgrid using optimized fuzzy logic controller considering economic dispatch. *Energies* **2019**, *12*, 1457. [[CrossRef](#)]
32. Sandels, C.; Widén, J.; Nordström, L. Forecasting household consumer electricity load profiles with a combined physical and behavioral approach. *Appl. Energy* **2014**, *131*, 267–278. [[CrossRef](#)]